Novel Materials from Clay and Functionalized Clay Nanoparticles: Application in Remediation of Lead, Cadmium and Pentachlorophenol from Water

Marikah David[1], Wanyika Harrison*[1] Gatebe Erastus[2]

[1]Department of Chemistry; Jomo Kenyatta University of Agriculture and Technology (JKUAT)

[2]Kenya Industrial Research and Development Institute (KIRDI)

Abstract— The importance of water purification especially removal of both organic and inorganic contaminants cannot be overemphasized, hence the need to develop water purification materials that are cheap, easily available and efficient. This would ensure realization of the Clean Water and Sanitation Sustainable Development Goal (SDGs). The current study involves isolation of clay nanoparticles (CNP) and functionalizing them with Cetylpyridinium Chloride (CPC) and Tetradecyltrimethylammonium Bromide (TTAB) to form C-CPC and C-TTAB respectively, so as to increase efficiency in removal of lead, cadmium and pentachlorophenol (PCP) through batch process. Clay was acquired locally, purified and CNP isolated by sedimentation and centrifugation. The CNP, C-CPC and C-TTAB were characterized using Fourier Transform Infra-Red (FTIR) spectroscopy, X-Ray Diffractometry (XRD), Scanning Electron Microscopy (SEM) and High Resolution Transmission Electron Microscopy (HRTEM). HRTEM revealed a particle size of 12-15 nm for the three adsorbents. CNP had a lead removal efficiency of 88% at initial concentration of 80 ppm and 94% for Cadmium at initial concentration of 50 ppm, while C-CPC and C-TTAB had lead removal efficiencies of 98%. For cadmium removal, C-CPC and C-TTAB had 98.2% and 98.6% efficiencies respectively. In pentachlorophenol (PCP) adsorption, CNP, C-CPC and C-TTAB had removal efficiencies of 85.6%, 87.7% and 84.6% respectively. The findings suggest that isolation of CNP and consequent modification with the surfactants increases adsorption efficiency of clay against the water pollutants.

Index Terms— CNP, C-CPC, C-TTAB, Lead, Cadmium, PCP and Adsorption

1.0 INTRODUCTION

Water purification is a process of great importance, since it helps in the removal of both organic and inorganic contaminants from water, thus rendering water safe for drinking and other portable uses [1]. Growth and development of sectors like production industry and agriculture have led to competition for fresh water resources with human population. These sectors have also contributed largely to pollution of the available water resources. This problem has been aggravated by the increasing human population and lack of sufficient rainfall in many parts of the world [2], hence the need to maintain or sustain the available water resources and purify waste water so that it can be reused. Water purification is a global practice and many convectional processes are being used for removal of organic and inorganic water contaminants. These methods include ion-exchange, precipitation, chemical coagulation, membrane separation, electroplating, sorption (adsorption and biosorption) and electro kinetics [1]. A lot of research work is being carried out on new and innovative methods of water purification, such as; reverse osmosis and supercritical water technology [3]. Among the purification methods mentioned, adsorption is considered as the most promising method due to its low cost of operation, ease of availability of adsorbents and its efficiency. Furthermore, other methods have a number of de-merits: high operational cost, poor efficiency, unavailability and generation of large amounts of sludge wastes [4]. Water may contain physical, chemical and biological contaminants which may have adverse effects on human health. Heavy metals are among chemical inorganic contaminants that are present in water. Although heavy metals have been known to have several adverse effects on human health as studied by international bodies like WHO, their usage in some parts of the world has increased especially in the developing or less developed countries [5]
Cadmium occurs in compounds such as color pigments, polyvinyl chloride products, rechargeable nickel–cadmium batteries, emissions from industries, fertilizers and sewage sludge coming into contact with water bodies or farming land and washed off to nearby water bodies by runoff. Its health effects include kidney damage, acute pulmonary effects, skeletal damage and cancer. The permissible limit of cadmium in water

is 0.003 ppm [6]. Lead exposure mainly occurs in mines and smelters where high levels in air emissions pollute areas adjacent to these industries, [6]. Another major lead exposure route is via paints since lead driers are used in paint formulation. Previously, lead was used as a fuel additive and fuel emissions were the major lead exposure routes to the environment, but with the introduction of unleaded fuels, lead exposure through fuel emissions has greatly decreased. Another main anthropogenic source of lead to environment is through pesticides. Toxic effects of lead may be seen on the gastrointestinal, renal and nervous systems. The target organs are brain, thyroid gland and kidneys. Lead permissible limit in water is 0.01 ppm [5]. Pentachlorophenol (PCP) is a compound under the organo chlorine group that finds application as a pesticide and disinfectant. Its molecular formulae is C_6HCl_5O and is mainly found as PCP sodium salt, which is soluble in water [7]. PCP has exposure health effects on kidney, blood, liver and immune system. It also causes acute leukemia. The permissible limit of pentachlorophenol is 0.001 mg/l, [8]

Clay is made up of silica and alumina (silicate of aluminum) and has many applications like ceramic making, catalysts, coating and paper industry, biosensors and as an adsorbent for heavy metals and when modified, adsorbent for organic molecules [9]. It has many minerals, over 400, but the ones that can be used as adsorbents and be synthesized to nano particles are kaolinite and montomorilonite (smectite) groups of clay minerals [9]. Smectite is a non-metallic clay with a monoclinic crystal structure and a general formula (Ca, Na, H) (Al, Mg, Fe, Zn) $_2$(Si, Al) $_4O_{10}$ (OH) $_2$ nH_2O. The various smectite types are montomorillonite, bentorite, nontronite, beidellite, saponite and hectorite. It is used as a sorbent in water purification by adsorption method since it possess a high specific surface area, chemical and mechanical stability, and a number of structural and surface properties i.e. the intergalley space placed between the silica tetrahedral sheet and alumina octahedral sheet contains exchangeable cations and tetrahedral silica sheet which is negatively charged as a result of isomorphic substitution of the cations. These two properties make clay nanoparticles (CNP) to be strong adsorbents for metal cations, [9]. Khalfa and Bagane [11] reported to have removed cadmium from aqueous solution using natural and activated clays and Darban [12] synthesized nano-alumina powder with high surface area of 201.53 m^2/g and small particle size of 22-36 nm from impure kaolin and used it for removal of arsenite from aqueous solutions, where he achieved an adsorption recovery of 97.65% from an initial arsenite concentration of 10 mg/l. Clay is highly hydrophilic and is converted to hydrophobic nature by functionalizing with organo modifiers which are quaternary ammonium salts, that possess a permanent positive charge. They undergo cation exchange with the cations in the intergallery space [13].

Cetylpyridinium Chloride (CPC) is a quaternary ammonium salt with a molecular formulae of $C_{12}H_{38}N$ Cl, and is highly soluble in water [14]. Liao min [15] reported a 78.81% removal percentage of acetochlor for organoclays made by surface modification of montomorillonite with CPC. Tetradecyltrimethylammonium Bromide (TTAB) is an organo modifier with molecular formulae of $C_{17}H_{38}N$ Br. Liao min [15] also reported TTAB-bentonite and TTAB-montomorillonite to have acetochlor removal percentages of 89.15% and 63.94% respectively.

Clay has previously been used in water purification as stated above. Kenyan clay has also been used for remediation of pollutants from water. In both occasions, micro sized clay was used. Isolation of CNP and surface modification with surfactants increases efficiency, thus achieving better results. The current study involves isolation of CNP from locally available clay and modification of the CNP with quaternary ammonium salts for removal of PCP, lead and cadmium from water.

2.0 MATERIALS AND METHODS

2.1 Isolation of Clay Nanoparticles

Clay soil was obtained from Jomo Kenyatta University of Agriculture and Technology (JKUAT) compound, in Juja, Kiambu County, Kenya ($1^0$05'23.214''S, $37^0$00'50.124''E). After collection, 100 gms of the clay soil was sieved through mesh no. 35 with a 420 µm opening, and treated with 1L of 10% H_2O_2 (Kobian Chemicals, 99.8% purity) followed by 1L of 0.5 M NaOH (Kobian Chemicals, 99.8% purity) to get rid of any organic materials, then washed with distilled water twice (to get rid of traces of H_2O_2 and NaOH) and dried in the oven at 80^0C for 24 hours. CNP were isolated through sedimentation and centrifugation according to [16]. After isolating CNP, modification was done using CPC and TTAB (Sigma-Aldrich, 99% purity) quaternary ammonium salts according to [17] method. The CNP CEC (Cation Exchange Capacity) was 89 meq/100 g and was determined using acetate method.

2.2 Characterization of Clay and Modified Clay Nanoparticles

Both clay and modified clay nano particles were characterized using various methods; Shimadzu 8400 series Fourier Transform Infrared (FTIR) spectrometer (400-4000 cm^{-1}) for functional groups determination, XPERT-PRO X-ray Diffraction (XRD) diffractometer with Gonio Scan Axis and Cu Kα (λ = 1.540 nm) radiation for determination of *d* spacing, Philips / FEI (XL30) Scanning Electron Microscope (SEM) and TECNAI F3OST-TEM High Resolution Transmission Electron Microscope (HR-TEM) for morphology and particle size investigation. Both SEM and TEM micrographs were analyzed using Pebbles software for particle size distribution, [18]

2.3 Adsorption Studies

One factor at a time method was used in adsorption studies where batch process experiments were set up each in triplicate. The stock solutions of lead, cadmium and PCP were prepared using Pb $(NO_3)_2$, Cd $(NO_3)_2.4H_2O$ and PCP Na salts (Kobian Chemicals Ltd, 99.8% purity) respectively. Percentage removal was calculated using equation 1 and quantity adsorbed at equilibrium using equation 2

$$\%\ Removal = \left(\frac{C_i - C_e}{C_i}\right) x\ 100 \text{ ----- Equation 1}$$

$$q_e = \frac{(C_i - C_e)}{M}\ x\ V \text{ ---------- Equation 2}$$

Where q_e is adsorbed quantity at equilibrium, C_i is initial concentration, C_e is final concentration, M is mass of the adsorbent and V is the volume of the solution.

2.3.1 Optimization of Lead, Cadmium and PCP Initial Concentration

Lead initial concentrations ranged from 10, 20, 40, 60, 80 and 100 ppm, cadmium from 10, 20, 50, 100, 150 and 250 ppm and 2, 4, 6, 8, 8 and 10 ppm for PCP. For lead and cadmium, a volume of 50 ml for each concentration was placed in a beaker, one gram of each adsorbent (CNP, C-CPC and C-TTAB) added, agitated for two hours at 100 rpm using rotary shaker then filtered using Whatmann filter paper No. 42 and then analyzed using Shimadzu AA 6200 Atomic Absorption Spectrometer (AAS). Lead concentrations were set at pH 4.56 and cadmium at pH 1.51. For PCP, 10ml of each was placed in a beaker, one gram of adsorbent added, equilibrated for 24 hours, then filtered with micro filter (0.45 µm) and analyzed using UFLC Shimadzu High Performance Liquid Chromatography (HPLC) with a SPD M20A Prominence Diode Array detector. HPLC conditions: Column (Supelco C18, 15cm x 4.6 mm, 5µm), temperature (30^0C), flowrate (10µl/min) and mobile phase (acetonitrile: water 65:35). Wavelength (284 nm)

2.3.2 Optimization of Lead, Cadmium and PCP adsorption Contact Time

Contact time was varied in the order 10, 30, 50, 100, 150 and 200 minutes for both lead and cadmium, and 2, 4, 8, 12 and 24 hours for PCP. For lead, initial concentration was set at 80 ppm, 100 ppm for cadmium and 10 ppm for PCP. One gram of each of the three adsorbents was added to each 50 ml solution, agitated at 100 rpm for each time interval, filtered using Whatmann filter paper No. 42 and analyzed using AAS as in 2.3.1. pH was set at 4.56 and 1.51 for lead and cadmium respectively. For PCP, a time interval of 2, 4, 8, 12 and 24 hours was used for the equilibration process, then filtered using micro filters (0.45 µm) and analyzed using HPLC as in 2.3.1.

2.4 Adsorption Isotherms

Adsorption isotherms help in determination of the adsorbed quantity and characteristics of the adsorption process.

2.4.1 Langmuir Isotherm

Data from optimization of initial concentration is fitted in Langmuir isotherm and if it fits, the adsorption reaction follows a monolayer process. Equation 3 illustrates the Langmuir isotherm. A plot of $\frac{1}{q_e}$ verses $\frac{1}{C_e}$ is drawn, where q_m and *b* are derived from the slope and intercept respectively.

$$\frac{1}{q_e} = \frac{1}{bq_m}\frac{1}{C_e} + \frac{1}{q_m} \text{ ---------- Equation 3}$$

Where b is Langmuir constant and q_m is maximum adsorbed quantity.

2.4.2 Freundlich Isotherm

Data from optimization of initial concentration is also fitted in freundlich isotherm and if it fits, the adsorption reaction follows a multilayer process. It is illustrated in equation 4, where a graph of $\ln q_e$ verses $\ln C_e$ is plotted, $\frac{1}{n}$ and K_f are derived from the slope and intercept respectively.

$$\ln q_e = \ln K_f + \frac{1}{n}\ln C_e$$ ---------- Equation 4

Where n constant is related to the intensity of adsorption energy and K_f is freundlich constant.

2.4.3 Flory-Huggins Isotherm

Flory-Huggins isotherm model is used in determination of the degree of surface coverage characteristic of adsorbate on the adsorbent. Equation 5 below depicts its representation where a graph of $\log {}^{\theta}/_{C_e}$ against $\log(1-\theta)$ is plotted. α_{FH} and K_{FH} are derived from the slope and intercept respectively

$$\log {}^{\theta}/_{C_e} = \log K_{FH} + \alpha_{FH}\log(1-\theta)$$ --------

Equation 5

Where α is the degree of surface coverage and K_{FH} is the Flory-Huggins constant.

2.5 Adsorption Rate Models

Rate models assist in describing how fast or slow the adsorption reaction takes place and the number of active sites present in the adsorbent.

2.5.1 Pseudo-first Order rate model

Data from the optimization of contact time is fitted in Pseudo-first order rate model and if it fits, the adsorbent has only one kind of active site. This model is represented by equation 6, where a graph of $\log(q_e - q_t)$ verses t is plotted. q_e and K_{p1} are derived from the intercept and slope respectively.

$$\log(q_e - q_t) = \log q_e - \frac{K_{p1}}{2.303}t$$ --- Equation 6

Where q_e is the amount adsorbed at equilibrium, q_t is amount adsorbed at time t and K_{p1} is pseudo-first order rate reaction.

2.5.2 Pseudo-second Order rate model

Data from the optimization of contact time is fitted in to Pseudo-second order rate model and if it fits, the adsorbent has more than one kind of active site. Equation 7 represents pseudo-second order rate model. A graph of $\frac{t}{q_t}$ verses t is plotted. q_e and K_2 are derived from the slope and intercept respectively.

$$\frac{t}{q_t} = \frac{1}{K_2}q_e^2 + \frac{1}{q_e}t$$ ---------- Equation 7

Where K_2 is the pseudo-second order rate constant.

3.0 RESULTS AND DISCUSSIONS

3.1 Clay Nanoparticles (CNP)

Clay nanoparticles were successfully isolated as confirmed by the HR-TEM images in figure 1 A. The average particle size was ~13.5 nm as shown in the histogram inset. Clay is made up of tetrahedron silica layers and octahedron alumina layers, but in figure 1 A, crystals with hexagonal shapes can be seen. This can be attributed to truncated octahedron (TO) shape, [19]. Figure 1 B and 1 C depict HRTEM images of C-CPC and C-TTAB, with an average particle size of ~14 nm. A closer look at figures 1 A, 1 B and 1 C, agglomeration can be seen in Figure 1 B and 1 C as a result of modification. The alkyl chains occupy the negatively charged clay surface, thus eliminating the repulsive electrostatic forces, leading to agglomerates formation, [20]. The modification process involved introduction of organic cations to the negatively charged clay surface, which are bonded strongly by electrostatic forces. The siloxane surface form van-der-waal interactions with alky chains of CPC and TTAB [21]. In the clay gallery space, modification could be attributed to intercalation via cation exchange since CPC and TTAB are quaternary ammonium salts with a permanent positive charge. Figure 2 shows the plausible modification schematic representation with the resulting orientation of micelle in the clay particle. This orientation could be attributed to loading occurring slightly in the gallery space and intensely in the siloxane surfaces, as a result of the surfactant molecule being too big to fit in gallery space, [22]. Figure 3 depicts the colorized SEM images of clay particles, CNP and 3D reconstruction images. These images were colorized and reconstructed using Mountain 7 software. The colorization is based on the shape and size of the particles. The 3D reconstruction images are created by reconstruction of four identical SEM micrographs. In figure 3 B and 3 D, the morphology of the clay particles can be seen to be rugged an indication that the clay particles and CNP did not have a definite shape. Figure 3 A is the SEM image (scale 100 µm) of the clay particles prior to sedimentation and centrifugation processes showing average particle sizes of ~56 µm. Figure 3 C is the SEM image after the isolation processes which

reveals average particle size of ~164 nm. This is a clear indication that the isolation processes greatly reduced the particle size distributions of the clay particles.

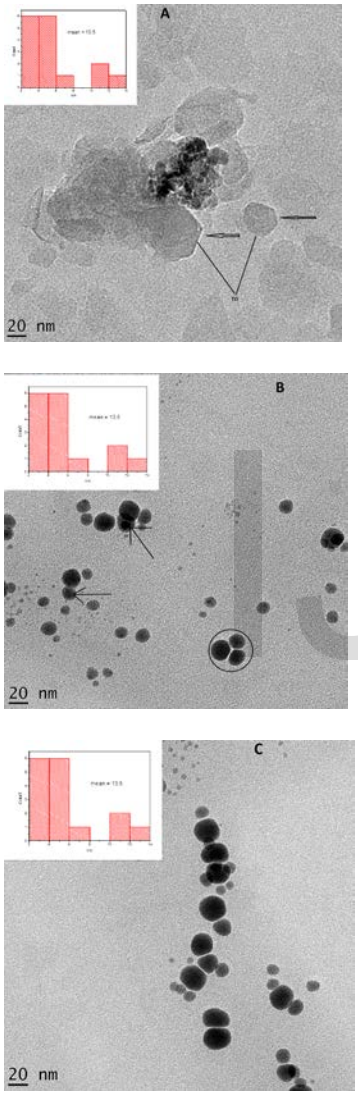

Figure 1: HR-TEM images of CNP (A), C-CPC (B) and C-TTAB (C). Inset, particle size distributions

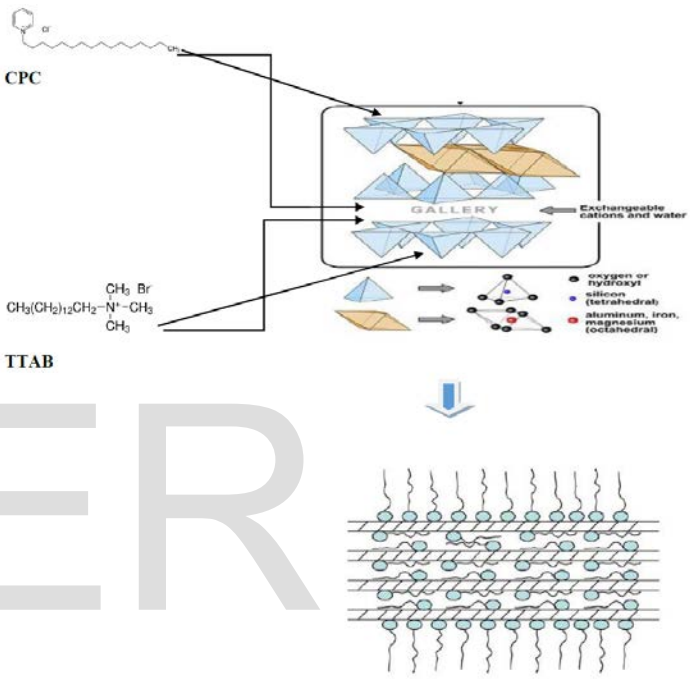

Figure 2: Schematic representation of modification of clay nanoparticles with of CPC and TTAB

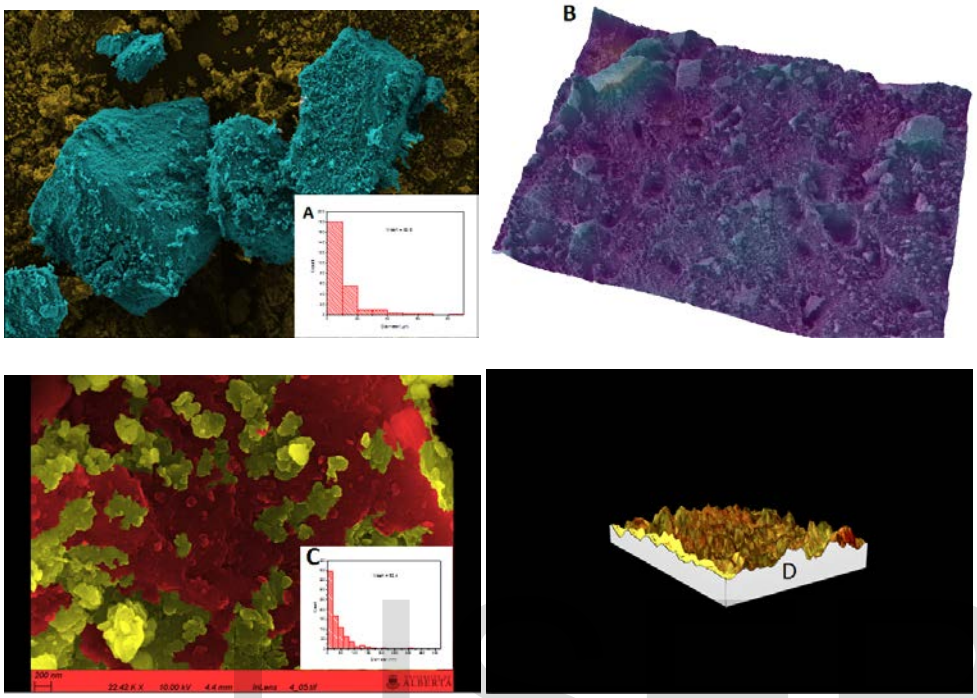

Figure 1. SEM images of clay particles (A), 3D reconstruction image of clay particles (B), SEM image of clay nanoparticle (C) and (D) 3D reconstruction image of clay nanoparticles. Inset is particle size distribution histograms

3.2 Characterization of Clay Nanoparticles (CNP) and Functionalized Clay nanoparticles (C-CPC and C-TTAB)

Fourier Transform Infra-Red (FT-IR) Spectroscopy was used to characterize the functional groups present in the three adsorbents as depicted in figure 4 and table 1. Maina [23] further discussed the CNP spectrum. In figure 4 A, the C-CPC spectrum shows CH_2 antisymmetric stretching at 2920.0 cm^{-1} and 2854.5 cm^{-1} for symmetric stretching of the same CH_2. The peak at 1477.4 cm^{-1} seen in the spectra of CPC and C-CPC can be attributed to bending vibrations of C-H fragments. The peak at 3062.7 cm^{-1} in the C-CPC spectrum is an indication of presence of a benzene ring since the peak is as a result of C-H stretching on the benzene ring.

In figure 3 B, 2923.6 and 2923.9 cm^{-1} depicts antisymmetric stretching of CH_2 for TTAB and C-TTAB respectively. Symmetric CH_2 stretching for both TTAB and C-TTAB are 2850.6 and 2854.5 cm^{-1} respectively. In TTAB spectrum, 1477.4 cm^{-1} is as a result of bending vibration of C-H fragments, which is also evident in C-TTAB spectrum at 1469.7 cm^{-1}. The presence of peaks of CPC and TTAB surfactants in the C-CPC and C-TTAB spectra respectively was an indication that modification had occurred. The absence of peaks in both C-CPC and C-TTAB spectra that were not present in CNP spectrum and could not be accounted for is an indication that the modification process followed physisorption process.

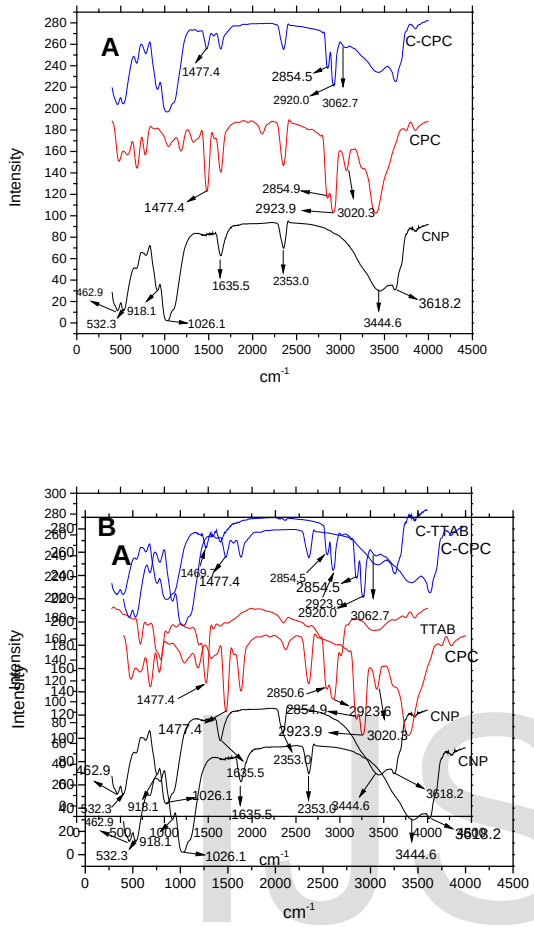

Figure 2: FTIR spectra of A (CNP, CPC and C-CPC) and B (CNP, TTAB and C-TTAB)

Table 1: FTIR peaks assignment for CNP spectrum

Frequency (cm^{-1})	Peak assignment
3620.1	Structural OH stretching
3442.7	Water OH stretching
1649.0	Water OH deformation
1035.7	Si-O stretching
914.2	Al-Al-OH deformation
790.8	Si-O quartz and silica stretching

X-ray Diffraction Spectroscopy (XRD) was used to confirm intercalation of the surfactants into the clay interlayer space (Figure 5). The XRD patterns depict peaks at 2θ: 19.89^0, 34.93^0 and 61.97^0 with hkl mirror indices (200), (222) and (531) respectively. Both (200) and (222) had body-centered lattice (bcc) and face-centered lattice (fcc). (531) had (fcc) [24]. A search of the acquired WXRD spectrum of CNP in CRYSTMET database, [25] revealed that these peaks and mirror indices are characteristic of Montmorillonite clay. Wanyika, (2014) in his research work did WXRD on pure Montmorillonite and reported peaks at 2θ: 20^0, 35^0 and 62^0. A closer look at peak 2θ 19.7^0 shows that there is an increase in the *d* spacing of CNP from 4.463 Å to 4.464 Å and 4.465 Å for C-CPC and C-TTAB respectively. The slight increase in the *d* spacing could be attributed to the alkyl chains of the surfactants assuming a C-C-C plane arrangement parallel to the layers in the intergallery space, [10]. This could be attributed to CPC and TTAB surfactant molecules being large and rigid. This is depicted in figure 2 and discussed in 3.1.

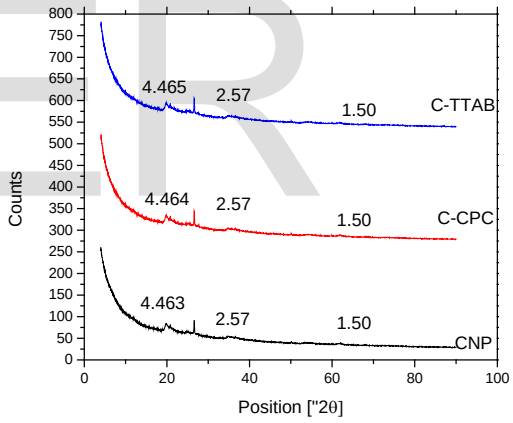

Figure 3: WAXRD patterns for CNP, C-CPC and C-TTAB

3.2 Adsorption Studies

3.2.1 Optimization of Initial Concentration

Figure 6 depicts the removal efficiency verses initial concentration graphs that were used in the initial concentration optimization adsorption studies of lead, cadmium and PCP. In figure 6 A for CNP adsorbent, as the initial concentration of lead increases, the removal efficiency increases. This could be attributed to competition of the siloxane and oxyhydroxyl active sites of CNP adsorbent [21] and exchangeable cations by the lead ions.

The initial lead concentration provides the force needed to overcome the mass transfer resistance from the liquid phase to the solid phase, hence an increase would automatically provide more force thus more removal efficiency [25]. For C-CPC and C-TTAB adsorbents, as the initial concentration increases, the removal efficiency decreases and this can be attributed to exhaustion of the adsorbents active sites by lead ions as the initial lead concentration increases. Figure 6 B depicts a removal efficiency verses initial cadmium concentration graph for CNP, C-CPC and C-TTAB adsorbents. It can be seen that as the initial concentration increases, the removal efficiency decreases and this can be attributed to exhaustion of the adsorbent active sites by the cadmium ions as the initial cadmium concentration. In lead adsorption using CNP, as the initial concentration increases, the removal efficiency increases, while for cadmium adsorption with the same adsorbent, a reverse trend is observed. This could be attributed to the smaller ionic radius of Cd^{2+} (0.97 Å) as compared to Pb^{2+} (1.19 Å) [27], thus can access inner sphere surface of clay by passing the siloxane ditrigonal cavity which is 1 nm in diameter [21], thus adsorption of Cd^{2+} will occur at inner and outer sphere surfaces of clay hence the high removal efficiencies in the initial stages and which depleted as initial concentration increases. Figure 6 C shows removal efficiencies verses initial PCP concentration graph for CNP, C-CPC and C-TTAB adsorbents. As the initial concentration increases, the removal efficiency increases, this is as a result of competition of the active sites of the three adsorbents by the PCP molecules. CNP revealed higher removal efficiency as compared to C-CPC and C-TTAB in the initial stages which could be attributed to the fact that when a phenol is dissolved in water, it forms a phenoxide which is acidic. If an electron withdrawing group is attached to the benzene ring, it increases the acidic by decreasing the negative charge of the phenoxide [28]. In the case of PCP, five chlorine atoms are attached to the phenol hence make it strongly acidic thus can attack the edge hydroxyl group (silanol) which are more active than the basal hydroxyl group [21]. As initial concentration increased to 6 ppm, both C-CPC and C-TTAB caught up with CNP due to the depletion of silanol active sites which caused a significant drop of removal efficiency at concentration 10 ppm. C-CPC and C-TTAB adsorption for PCP was via partition process where the alkyl chains of the CPC and TTAB surfactants partitioned with the PCP molecules [15]. Functionalization brought about increment in the gallery space hence the PCP molecules could be trapped in the gallery space.

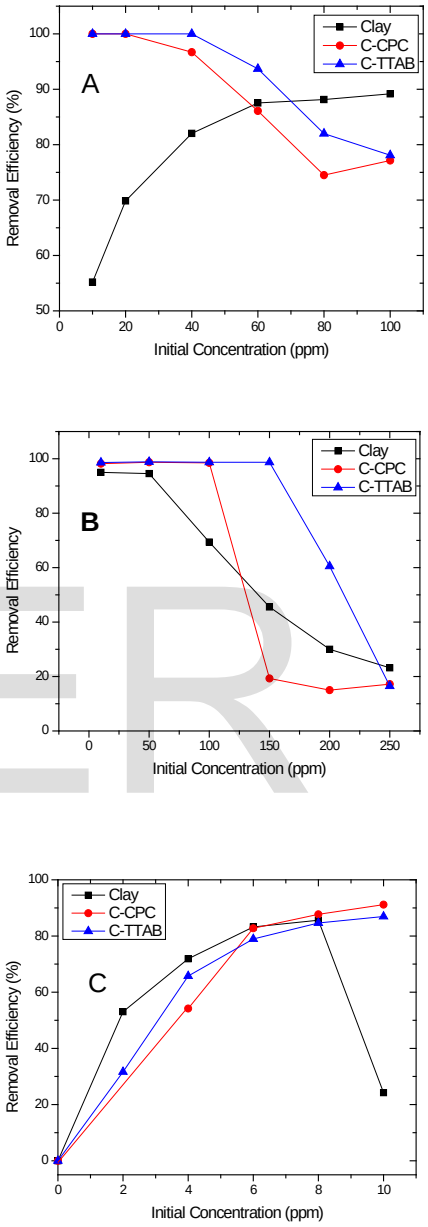

Figure 4: Removal efficiency (%) verses Initial concentration graphs for Lead (A), Cadmium (B) and PCP (C) using CNP, C-CPC and C-TTAB

3.3 Adsorption Isotherms

3.3.1 Langmuir and Freundlich Isotherms

Figure 7 A represent Langmuir isotherm for lead adsorption and 8 A freundlich isotherm for lead adsorption. A comparison of R^2 values from table 2 (Langmuir values) and 3 (Freundlich values), freundlich R^2 value are close to 1 than Langmuir values hence the adsorption process best fitted in the Freundlich isotherm model implying it followed a multi-layer process. For CNP, since 1/n is above unity, a convex Freundlich can be used to characterize the adsorption process, while for both C-CPC and C-TTAB; a convex Freundlich cannot be used since 1/n was below unity [27]. In cadmium adsorption isotherm studies (figures 7 B and 8 B), comparison of R^2 values of langmuir and Freundlich from table 2 and table 3 respectively, Langmuir R^2 values are close to 1 than Freundlich's. This implies the adsorption process best fitted in the Langmuir isotherm model hence followed a mono-layer process. CNP, C-CPC and C-TTAB q_m were 3.77, 23.91 and 66.36 mg/g respectively. CNP had the least q_m while C-TTAB had the most, an indication that C-TTAB adsorbed more cadmium ions than CNP. This could be due to increased pH as a result of TTAB basic group intercalation [21], and Cd^{2+} adsorption is favored in basic pH, [26]. In PCP adsorption isotherms studies (figures 7 C and 8 C), a closer look at R^2 values for Langmuir and Freundlich, CNP had both R^2 values which were far away from 1 hence could not ascertain which isotherm fitted best. A closer look at freundlich's *n* value (10), the adsorption reaction is feasible since according to [29], if the n value is ($2 < n \leq 10$) the adsorption reaction is feasible. C-CPC and C-TTAB adsorption reactions fitted well in Freundlich isotherm since the R^2 was close to 1 than R^2 of Langmuir isotherm thus the adsorption process followed a multilayer process. This could be attributed to the layer formed during modification; hence after adsorbing PCP molecules, another layer was formed hence following a multilayer process.

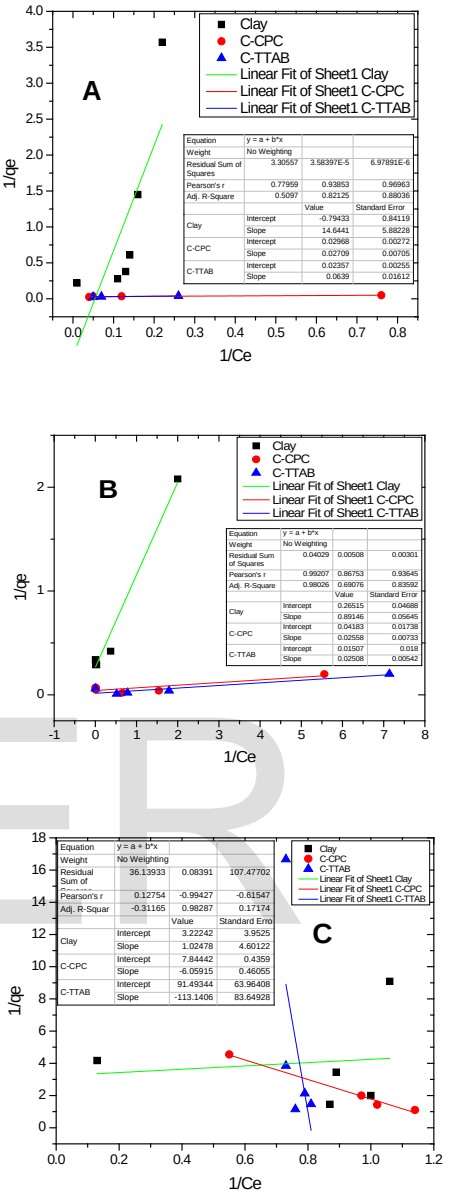

Figure 5: Langmuir Isotherm models for: A (Lead), B (Cadmium) and C (PCP)

Table 2: Langmuir Isotherm constants and values

	R^2	q_m	*b*
CNP (Lead)	0.7796	1.26	0.05
C-CPC (Lead)	0.9385	33.69	1.10
C-TTAB (Lead)	0.9696	42.43	0.36
CNP(Cadmium)	0.9921	3.77	3.30
C-CPC(Cadmium)	0.8675	23.91	0.75
C-TTAB(Cadmium)	0.9365	66.36	1.5
CNP (PCP)	0.1275	0.31	3.16
C-CPC(PCP)	0.9756	0.13	1.27
C-TTAB (PCP)	0.6155	0.01	0.88

Table 3 Freundlich Isotherm constants and values

	R^2	K_F	1/n	n
CNP (Lead)	0.9722	2.24 x 10^{-3}	3.28	0.305
C-CPC (Lead)	0.9396	18.17	0.20	5
C-TTAB (Lead)	0.9918	21.54	0.18	5.56
CNP (Cadmium)	0.8243	0.99	0.26	3.85
C-CPC (Cadmium)	0.1578	592.52	0.04	25
C-TTAB (Cadmium)	0.1746	1295.99	0.07	14.29
CNP (PCP)	0.1268	0.32	0.10	10
C-CPC (PCP)	0.9967	0.64	0.55	1.82
C-TTAB (PCP)	0.6925	24.70	16.15	0.06

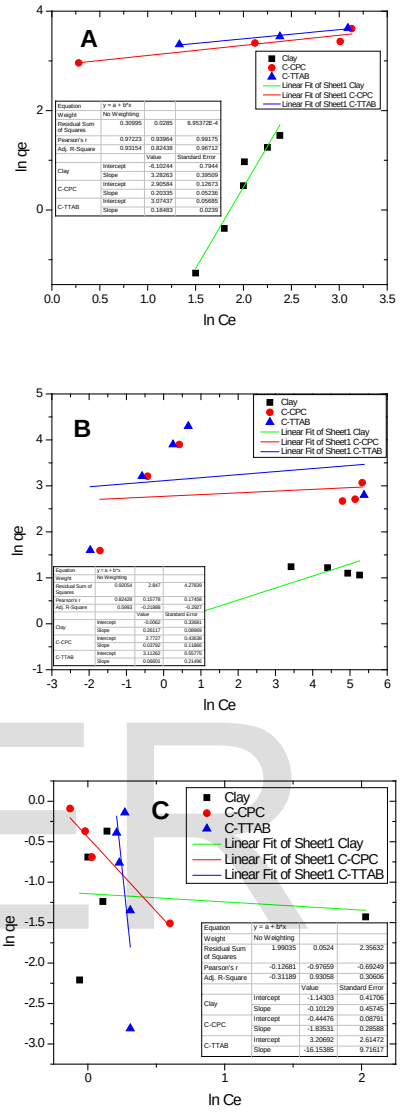

Figure 6 Freundlich Isotherm models for A (Lead), B (Cadmium) and C (PCP)

3.3.2 Flory-Huggins Isotherm

Figure 9 shows Flory-Huggins isotherm model that is used to describe the surface coverage of the adsorbate molecules on to the adsorbent particles. For lead, (figure 9 A) CNP had 0.20 α_{KF} which is below unity, while C-CPC and C-TTAB was 1.51, which is above unity, thus implying more lead ions were adsorbed by C-CPC and C-TTAB compared to CNP which could be attributed to the increase in the gallery space hence Pb^{2+} could access the inner sphere surface as discussed in 3.2.1. In cadmium adsorption (figure 9 B) all α_{KF} values were above unity which could be attributed to the adsorption reactions following a mo-

nolayer process as discussed in 3.3.1, hence the cadmium ions covered expansive surfaces of the three adsorbents. Figure 9 C depicts PCP adsorption where α_{KF} values for CNP, C-CPC and C-TTAB were 1.8, 0.76 and 0.64 respectively. CNP had 1.8 α_{KF} which is above unit and can be attributed to the higher removal efficiency in the initial stages as discussed in 3.2.1. C-TTAB had the lowest α_{KF} (0.64) which was below unit and could be attributed to the adsorption reaction being a multilayer process as indicated in 3.3.1.

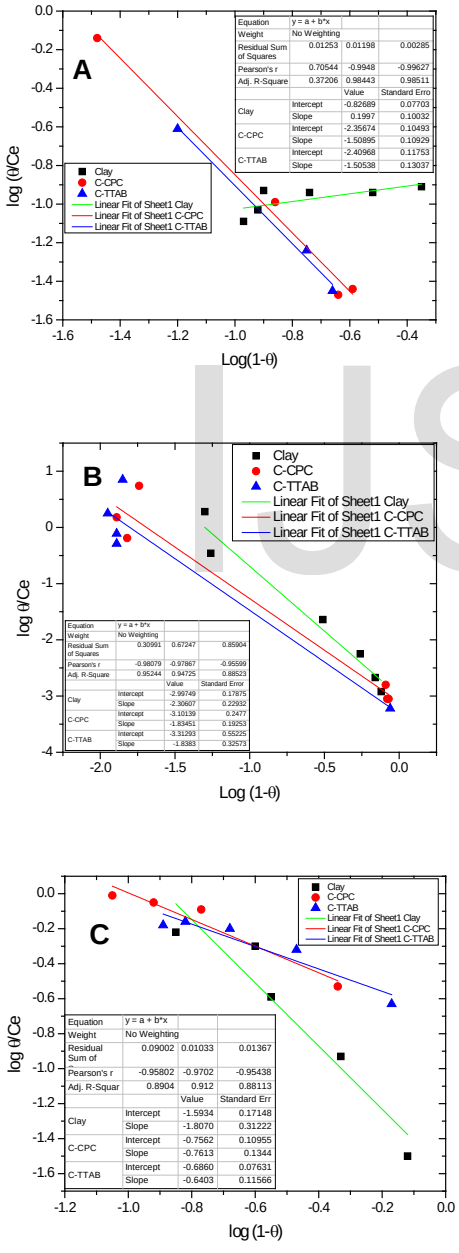

Figure 7: Flory-Huggins Isotherm models A (Lead), B (Cadmium) and C (PCP)

Table 4: Flory-Huggins isotherm constants and values

	R^2	K_{FH}	α_{KF}
CNP (Lead)	0.7054	0.14	0.20
C-CPC (Lead)	0.9948	4.4×10^{-3}	1.51
C-TTAB (Lead)	0.9963	3.89×10^{-3}	1.51
CNP (Cadmium)	0.9808	1.0×10^{-3}	2.30
C-CPC (Cadmium)	0.9787	7.92×10^{-4}	1.83
C-TTAB (Cadmium)	0.9560	4.86×10^{-4}	1.84
CNP (PCP)	0.9580	0.03	1.8
C-CPC (PCP)	0.9702	0.18	0.76
C-TTAB (PCP)	0.9544	0.21	0.64

3.4 Optimization of Contact Time

Figure 10 depicts the removal efficiency verses contact time graphs that were used in the contact time optimization adsorption studies of lead, cadmium and PCP. Figure 10 A shows removal efficiency verses contact time for lead by the three adsorbents at different contact times. It can be observed that from 0 to 20 minutes, there is a sharp increase in the removal efficiency which can be attributed to the availability of more active sites [25] of the CNP and C-CPC. C-TTAB exhibited a higher removal efficiency at 10 minutes than at 20 minutes which could be attributed to the initial competition of active sites hence the higher removal efficiency. From 20 minutes to 50 minutes the removal efficiency increased gradually as a result of gradual exhaustion of the active sites [25]. The graph tends to flatten from 50 minutes thus the optimum contact time is 50 minutes for CNP and C-TTAB. For C-CPC there was an increase in removal efficiency from 100 to 150 minutes, hence the optimum contact time is at 150 minutes. In figure 10 B (cadmium adsorption), the graph follows an increasing trend as the contact time increases from 10 minutes to 30 minutes. This can be attributed to the fact that as you increase contact time between the adsorbate (Cd^{2+}) and adsorbent (CNP, C-CPC and C-TTAB), more adsorption will take place. Beyond 30 minutes, the removal efficiency flattens indicating that initially, the number of active sites of the adsorbents was large but as time increases, there was exhaustion in the number of active sites hence the flat-

tening [25]. For PCP adsorption (figure 10 C), in all three adsorbents (CNP, C-CPC and C-TTAB) as time increased, the removal efficiencies increased. This could have been attributed to more contact time for adsorbents and PCP molecules hence the trend. CNP revealed high removal efficiency as compared to C-CPC and C-TTAB adsorbents. This could be as a result of competition for the only one kind of the active site (silanol) in CNP as compared to the more kinds of active sites (enlarged gallery space and alkyl chains of surfactants) in C-CPC and C-TTAB, [21]

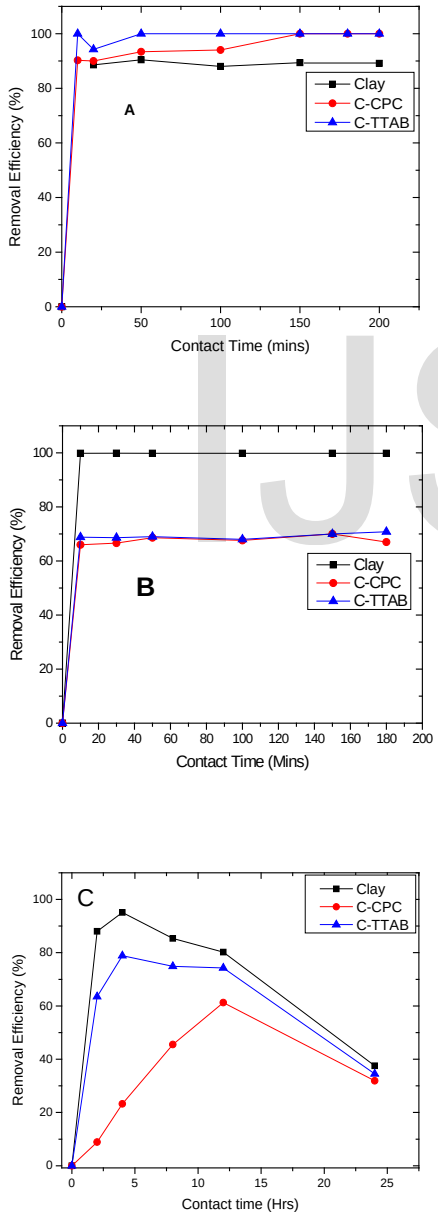

Figure 8: Removal Efficiency verses Contact time graphs for A (Lead), B (Cadmium) and C (PCP)

3.5 Adsorption Rate Models

3.5.1 Pseudo-First Order and Pseudo-Second Order Rate Models

Lead and cadmium rate models studies are illustrated in figure 11 (11 A and 11 B for lead and cadmium respectively) for pseudo-first order and figure 12 (12A and 12 B for lead and cadmium respectively) for pseudo-second order. A comparison of R^2 values in table 5 (Pseudo first order) and table 6 (Pseudo second order), pseudo second order R^2 values are close to 1 than for pseudo first order, hence the contact time optimization data best fitted well in this rate model. This implies that CNP, C-CPC and C-TTAB have more than one adsorption sites. For CNP, the sites are exchangeable cations present in the intergallery space and the negatively charged surface as a result of isomorphic substitution and the silanol groups [21]. For C-CPC and C-TTAB, the active sites are the inner sphere surface of clay as discussed in 3.2.1 and the alkyl chains of the modifiers, where adsorption is via complexion, [30]. The initial rate constant of the adsorption process was found to be highest for C-TTAB and lowest for CNP, an indication that adsorption was faster in C-TTAB and slower in CNP. This was the rate determining step. For PCP adsorption rate model studies (figure 11 C for pseudo-first order and 12 C for pseudo-second order), a comparison of R^2 values of pseudo first order and pseudo second order, CNP data fitted well in pseudo first order rate model, implying that it has one kind of active site (silanol groups) as discussed in 3.2.1. C-CPC and C-TTAB data fitted well in pseudo second order rate model hence had more than one kind of active sites (trapping of PCP molecules by the enlarged gallery space and partition of PCP molecules by alkyl chains of surfactants) as discussed in 3.3.1. All the h values for all the three adsorbent from pseudo second order rate model were very low, which could be attributed to the contact time interval series used.

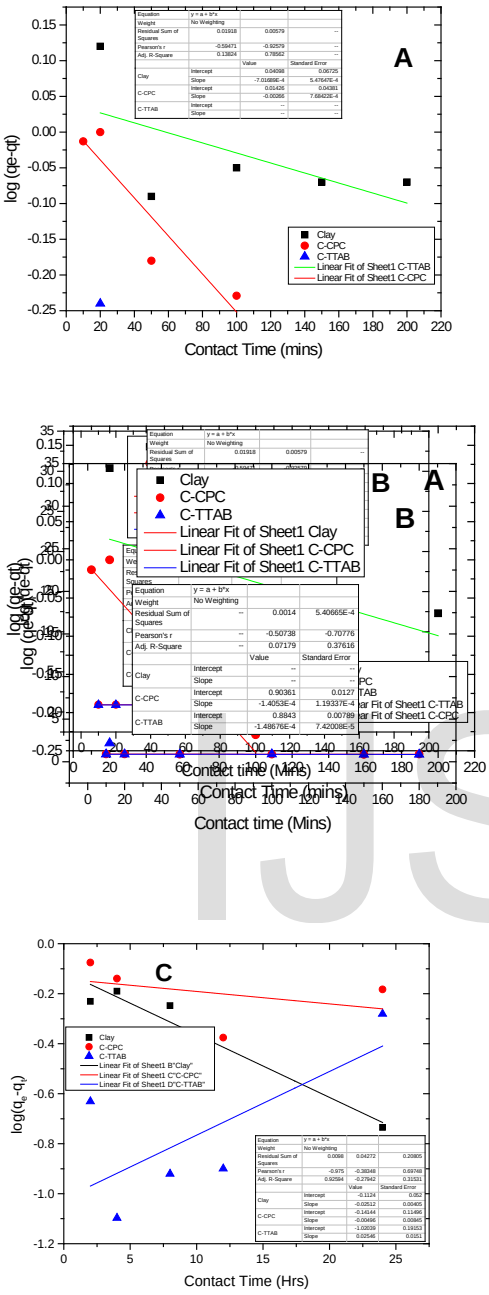

Figure 9:Pseudo-First Order Rate models for A (Lead), B (Cadmium) and C (PCP)

Table 5 Pseudo-First Order Rate model constants and values

	R^2	K_{p1}	q_e
CNP (Lead)	0.5947	1.61×10^{-3}	1.10
C-CPC (Lead)	0.7858	6.13×10^{-3}	1.03
C-TTAB (Lead)	-	-	-
CNP (Cadmium)	-	-	-
C-CPC (Cadmium)	0.5074	3.22×10^{-4}	8.00
C-TTAB (Cadmium)	0.7078	3.45×10^{-4}	7.66
CNP (PCP)	0.9259	0.07	1.07
C-CPC (PCP)	0.2794	0.01	1.01
C-TTAB (PCP)	0.3153	0.69	2.00

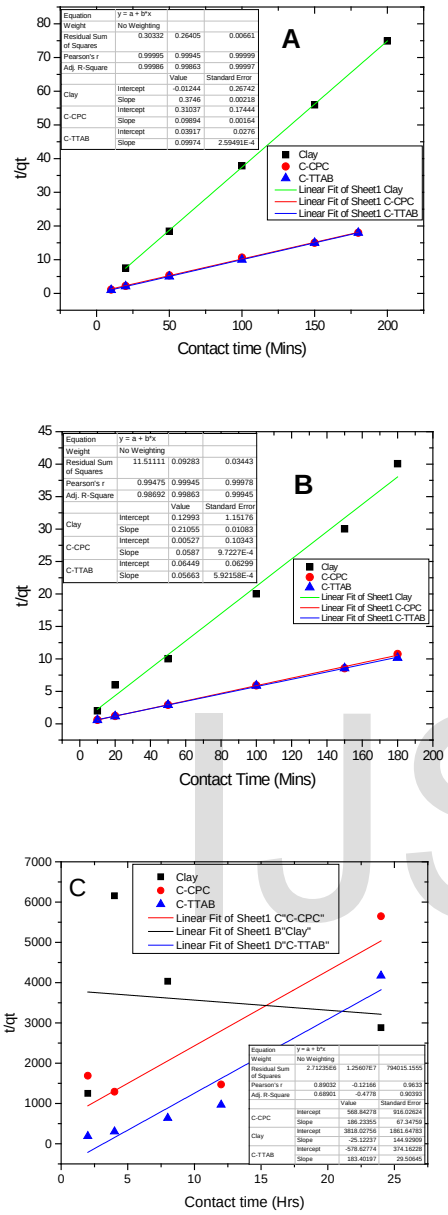

Figure 10 Pseudo Second Order Rate model A (Lead), B (Cadmium) and C (PCP)

Table 6 Pseudo Second Order Rate model constants and values

	R_2	q_e	K_2	H
CNP (Lead)	0.9999	2.67	573.06	4085.29
C-CPC (Lead)	0.9995	10.19	334.56	34,739.41
C-TTAB (Lead)	0.9999	10.03	2568.32	258,375.30
CNP (Cadmium)	0.9948	4.75	173.63	3917.53
C-CPC (Cadmium)	0.9995	17.04	5509.68	1,599,799.5
C-TTAB (Cadmium)	0.9978	17.66	4836.10	1,508,201.6
CNP (PCP)	0.1217	0.04	4.19×10^{-8}	6.70×10^{-11}
C-CPC (PCP)	0.8903	0.005	4.3×10^{-8}	1.08×10^{-11}
C-TTAB (PCP)	0.9633	0.005	4.3×10^{-8}	1.08×10^{-11}

4.0 Conclusions

In this study, CNP of average particle size of ~13.5 nm were isolated. Functionalization using CPC and TTAB surfactants was successfully carried out and confirmed by increment of *d* spacing of CNP from 4.463 Å to 4.464 Å and 4.465 Å for C-CPC and C-TTAB respectively. The presence of both CPC and TTAB peaks in the FT-IR spectra of C-CPC and C-TTAB further confirmed modification. CNP, C-CPC and C-TTAB revealed good adsorption capacities; CNP (0.20, 3.77 and 0.13 mg/g for lead, cadmium and PCP respectively), C-CPC (33.69, 23.77 and 0.13 mg/g for lead, cadmium and PCP respectively) and C-TTAB (42.43, 66.36 and 0.01 mg/g for lead, cadmium and PCP respectively). These adsorption capacities compared relatively well with the capacities of activated carbon (27.5-120, 30 and 8 mg/g for phenol, lead and cadmium respectively), a convectional adsorbent used in water purification. C-CPC and C-TTAB depicted high adsorption capacities for lead and cadmium which could be attributed to the functionalization process. CNP exhibited high adsorption capacity for PCP molecules which could be as a result of the reduction of the phenoxide negative charge by the five chlorine groups in the benzene ring and subsequence attraction to the silanol groups in the clay surface. Based on results from this study, CNP, C-CPC and C-TTAB show good potential as nano adsorbents for remediation of lead, cadmium and PCP from water.

Conflict of Interest

All authors declare that there is no conflict of interests in publishing this paper.

Acknowledgements
The authors are grateful to Jomo Kenyatta University of Agriculture and Technology, Nairobi, Kenya for funding the research project.

References

[1]. Mehdizadeh S., Sadjadi S., Ahmadi S. J., and Outokesh, M. (2014). Removal of heavy metals from aqueous solution using platinum nanopartcles/Zeolite-4A. *Journal of Environmental Health Science and Engineering*, 12(1): 1-7.

[2]. Alhawas, M., Alwabel, M., Ghoneim, A., Alfarraj, A., & Sallam, A. (2013). Removal of nickel from aqueous solution by low-cost clay adsorbents. *Proceedings of the International Academy of Ecology and Environmental Sciences*, *3*(2): 160.

[3]. Di Giacomo G. and Taglieri L. (2012). Supercritical Water Technology Applied to the Purification of Waters Contaminated by Toxic Micro-Polluting Organic Compounds. *Journal of Water Resource and Protection* **4:** 460.

[4]. Manohar D. M., Noeline B. F. and Anirudhan T.S. (2006). Adsorption performance of Al-pillared bentonite clay for the removal of cobalt (II) from aqueous phase. *Applied Clay Science* 31: 194–206.

[5]. Lars J. (2003). Hazards of heavy metal contamination. *British medical bulletin*. 68(1): 167-182.

[6]. Gautam, R. K., Sharma, S. K., Mahiya, S., & Chattopadhyaya, M. C. (2014). Contamination of heavy metals in aquatic media: transport, toxicity and technologies for remediation, 1-24.

[7]. Baselt R. (2008) Disposition of Toxic Drugs and Chemicals in Man, 8th edition, *Biomedical publications*, Foster City, California, pp. 1197-1200.

[8]. Fiege, H., Voges, H. W., Hamamoto, T., Umemura, S., Iwata, T., Miki, H.,. & Paulus, W. (2000). Phenol derivatives. *Ullmann's Encyclopedia of Industrial Chemistry*. Pp 102-140

[9]. Liu P. and Zhang L. (2007). Adsorption of dyes from aqueous solutions or suspensions with clay nano-adsorbents. *Separation and Purification Technology* 58(1): 32-39.

[10]. Xi, Y., Ding, Z., He, H., & Frost, R. L. (2004). Structure of organoclays—an X-ray diffraction and thermogravimetric analysis study. *Journal of colloid and interface science*, *277*(1), 116-120.

[11]. Khalfa L. and Bagane M. (2011). Cadmium Removal from Aqueous Solution by a Tunisian Smectitic Natural and Activated Clay: Thermodynamic Study. *Journal of Encapsulation and Adsorption Sciences* (1):65-71.

[12]. Darban A. K., Kianinia Y. and Taheri-Nassaj E. (2013). Synthesis of nano-alumina powder from impure kaolin and its application for arsenite removal from aqueous solutions. *Journal of Environmental Health Science and Engineering* 11 (1): 1.

[13]. Djebbar M., Djafri1 F., Bouchekara M. and Djafri A. (2012). Adsorption of phenol on natural clay. *African Journal of Pure and Applied Chemistry* 6(2): 15-25, 15.

[14]. Haps, S.; Slot, D. E.; Berchier, C. E.; Van Der Weijden, G. A. (2008). The effect of cetylpyridinium chloride-containing mouth rinses as adjuncts to toothbrushing on plaque and parameters of gingival inflammation: A systematic review". *International Journal of Dental Hygiene* 6 (4): 290–303

[15]. Liao Min. (2004) "Adsorption of phenthoate and acetochlor from water by clays and organoclays." *Journal of Environmental Sciences* 16, 5: 738-741.

[16]. Wanyika, H. (2014). Controlled release of agrochemicals intercalated into montmorillonite interlayer space. *The Scientific World Journal* (2014): 1-9

[17]. Zuzana N., Petr W., Lenka V. and Věra S. (2007). Sorption of alkylammonium cations on montomorillonite. *Actantic Geodynamic Geomater* 3 (147): 59-65

[18]. Mondini S., A. M. Ferretti, A. Puglisi, A. Ponti (2012). "Pebbles and Pebble Juggler: Software for Accurate, Unbiased, and Fast Measurement and Analysis of Nanoparticle Morphology from Transmission Electron Microscopy (TEM) Micrographs", *Nanoscale*, 4: 5356-5372

[19]. Wang, Z. L. (2000). Transmission electron microscopy of shape-controlled nanocrystals and their assemblies. *The Journal of Physical Chemistry B*, *104*(6), 1153-1175.

[20]. Zhou, L., Chen, H., Jiang, X., Lu, F., Zhou, Y., Yin, W., & Ji, X. (2009). Modification of montmorillonite surfaces using a novel class of cationic Gemini surfactants. *Journal of colloid and interface science*, *332*(1), 16-21.

[21]. Kurniawan, A., Ismadji, S., Soetaredjo, F. E., & Ayucitra, A. (2014). Natural Clays/Clay Minerals and Modified Forms for Heavy Metals Removal. *Heavy Metals In Water: Presence, Removal and Safety*, chapter 11, pp 213-220.

[22]. Egbuchunam, T. O., Obi, G., Okieimen, F. E., & Tihminlioglu, F. (2015). Effect of exchanged surfactant cation on the structure of kaolinitic clay. *Journal of Materials Science and Applications*, (2015): 1-14

[23]. Maina, E., Wanyika, H., Gachanja, A., & Marika, D. (2016). Instrumental Characterization of Montmorillonite Clays by X-ray Fluorescence Spec-

troscopy, Fourier Transform Infra-red Spectroscopy, X-ray Diffraction and UV/Visible Spectrophotometry. *Journal of Agriculture Science and Technology*, 17(1).

[24]. Smart, L. E., & Moore, E. A. (2012). *Solid state chemistry: an introduction*. CRC press, chapter 2, pp 75-132

[25]. Omorogie, M. O., Babalola, J. O., Unuabonah, E. I., & Gong, J. R. (2014). Hybrid materials from agro-waste and nanoparticles: Implications on the kinetics of the adsorption of inorganic pollutants. *Environmental technology*, *35*(5): 611-619.

[26]. Bhattacharyya, K. G., & Gupta, S. S. (2008). Kaolinite and montmorillonite as adsorbents for Fe (III), Co (II) and Ni (II) in aqueous medium. *Applied Clay Science*, *41*(1), 1-9.

[27]. Horsfall, M., & Spiff, A. I. (2005). Equilibrium sorption study of Al^{3}+, Co^{2}+ and Ag+ in aqueous solutions by fluted pumpkin (Telfairia occidentalis HOOK f) waste biomass. *Acta chimica slovenica*, *52*(2), 174-181.

[28]. Gallard, H., & Von Gunten, U. (2002). Chlorination of phenols: Kinetics and formation of chloroform. *Environmental Science & Technology*, *36*(5), 884-890.

[29]. Do D. D. (1998). Adsorption Analysis: Equilibria and Kinetics, *Imperial College Press, London*, 1st edition, chapter 2, pp 11-48.

[30]. Park M, Kim YC, Lee DH, Choi CL, Choi J, Lee S-R, Choy J-H (2004). Intercalation of Magnesium–urea complex into swelling clay. *Journal of Physical and Chemical. Solids* 65: 409-41.

- *Author (David Marikah) currently pursuing masters degree program in Chemistry in Jomo Kenyatta University of Agriculture and Technology, Kenya, E-mail: davidmarikah@gmail.com*
- *Co-Author (Harrison Wanyika) is currently a Doctor in Chemistry department in Jomo Kenyatta University of Agriculture and Technology (JKUAT), Kenya, E-mail: hwanyika@gmail.com*
- *Co-Author (Erastus Gatebe) is currently a Professor of Chemistry in Kenya Industrial Research and Development Institute (KIRDI), Kenya, E-mail: egatebe@gmail.com*